J Nanopart Res (2020) 22:92
https://doi.org/10.1007/s11051-020-04815-9

RESEARCH PAPER

Buckling response of functionally graded nanoplates under combined thermal and mechanical loadings

Ma'en S. Sari · S. Ghaffari · S. Ceballes · A. Abdelkefi

Received: 17 September 2019 / Accepted: 12 March 2020

Abstract This effort focuses on a buckling analysis of a functionally graded (FG), thin, rectangular nanoplate subjected to biaxial linearly varying mechanical loads and various temperature distributions through the thickness of the nanoplate. On the basis of the Eringen's nonlocal elasticity theory and Kirchhoff's classical plate theory, the governing equations are obtained for functionally graded rectangular nanoplates using the minimum total potential energy principle. In the proposed model, it is assumed that the mechanical and thermal properties of nanoplates are position-dependent and that they vary through the thickness via a power rule of the volume fraction of the constituents. The governing equation and boundary conditions are discretized for the rectangular nanoplate by adopting the Chebyshev spectral collocation method, and the resulting eigenvalue problem is solved to obtain the critical buckling loads. Finally, numerical results are presented to show the impact of various thermal loadings and boundary conditions on the buckling behaviors of size-dependent functionally graded nanoplates. Moreover, the influences of varying different parameters, such as the nonlocal parameter, power law index, temperature rise, aspect ratio, and slopes of the linearly varying axial mechanical forces, are investigated and discussed in detail. The study of each of these parameters highlights phenomena present at the nanoscale from a theoretical point of view.

Keywords Nanoplate · Thermal/mechanical loadings · Buckling · Nonlocal elasticity · Functionally graded · Biaxial loads

This article is part of the topical collection: *Nanotechnology Convergence in Africa*

Guest Editors: Mamadou Diallo, Abdessattar Abdelkefi, and Bhekie Mamba

M. S. Sari (✉)
Department of Mechanical and Maintenance Engineering, German Jordanian University, Amman 11180, Jordan
e-mail: maen.sari@gju.edu.jo

S. Ghaffari · S. Ceballes · A. Abdelkefi
Department of Mechanical and Aerospace Engineering, New Mexico State University, Las Cruces, NM 88003, USA

Introduction

Nanoelectromechanical systems (NEMS) have superior mechanical, physical, electrical, and thermal properties that distinguish them from other structures. NEMS are used in numerous systems applicable to the medical industries, generators, spintronics, resonators, sensors, energy harvesters, and transducers. Recently, due to the rapid development of the nanotechnology along with the need of equipment miniaturization, nanotubes, nanowires, and thin-films composed of specific materials have been introduced as the cornerstone for the manufacturing and fabrication of different nanostructures (Ansari and Gholami 2016). In order to analyze, model, fabricate, and design such nanosystems, it is crucial to increase the level of the understanding and insight about the different characteristics of small-scale structures. Furthermore, the main thermomechanical

Published online: 16 April 2020

challenge with thin nanoplates is to ensure structural stability in the presence of large and fluctuating stress states during fabrication and operation at elevated temperatures and pressures that in turn may lead to buckling, cracks, and fracture. Inaccurate modeling of nanostructures under mechanical and thermal loads may result in devices with low performance and efficiency.

It is known that nanotechnology techniques have been continuously applied to enhance the properties of such structures. For instance, Chen et al. introduced a method to increase the thermal conductivity of polymer matrix composites using hybrid filler that consists of carbon nanotubes and graphene nano-platelets. It was shown that a great increase has been achieved in the thermal conductivity for these materials (Chen et al. 2019). Additionally, for structures at the nanoscale, molecular dynamics has been utilized to analyze some observations. For example, the molecular dynamics has been used in modeling the nano-manipulation process based on atomic force microscope. Several factors were included as initial impact of nanoparticles, contact mechanics, and roughness (Korayem and Khaksar 2020).

As the nanoplates are extremely small, the experiments to investigate the behaviors of these structures are quite challenging. It is known that there are two main approaches for simulating the characteristics of the nanostructures: molecular dynamics (MD) simulation and continuum mechanics. The MD approach has been widely applied for simulating the different properties of nanostructures; however, this method is time-consuming and computationally expensive. On the other hand, elastic continuum model has been considered as an efficient method for examining the behavior of nanostructures. The classical continuum theories are scale free; therefore, they cannot handle the small-scale effect on the different properties for these nanostructures. Thus, these theories are insufficient in describing the behaviors of nanostructures. For the sake of applying the continuum model in the analysis of the nanostructures, realistic amendments that incorporate the small-scale effect should be introduced. Hence, few theories have been proposed as the modified coupled stress theory, the strain gradient theory, and the nonlocal elasticity theory that will be used in this study to investigate the buckling behavior of nonlocal Kirchhoff plates subjected to both biaxial and thermal loads.

Functionally graded materials (FGMs) are a novel generation of composite materials composed of two or more different materials in which the properties vary smoothly between the interfaces of the materials. FGMs were initiated by a group of Japanese scientists in 1984 during a space plane project (Koizumi 1997). Due to their superior properties and excellent performance under mechanical loadings in high temperature environments, beams and plates composed of FGMs have been widely applied in modern industries including aeronautic/astronautic manufacturing industry, defense industry, biomedical sectors, engine combustion chambers, vehicle industry, ship engineering, nuclear engineering, and reactors in the last few decades (Akbaş 2017; Kolahchi et al. 2015). Various fabrication techniques are used for FGMs, such as eliminating the interface, inducing non-uniform distributions of dispersoids in a homogeneous particle composite, and sequential buildup of layers.

Nanoscale structures, which are often made of FGMs, have recently attracted great attention for engineering and technology fields (Rahmani and Jandaghian 2015; Ghadiri et al. 2016; Norouzzadeh et al. 2017; Akbarzadeh Khorshidi et al. 2017; Hosseini et al. 2016). Thus, FGM nanoplates have been investigated by many researchers to understand their mechanical behaviors in the most recent years (Yuan et al. 2020; Lori Dehsaraji et al. 2020; Żur et al. 2020; Ruocco and Reddy 2020; Guo et al. 2020). Reviewing predictions for the static and dynamic behaviors of plates and nanoplates, there have been several studies investigating static and dynamic behaviors of these structures (Karami et al. 2018; Sahmani et al. 2014; Liu et al. 2019; Arefi et al. 2018; Farajpour et al. 2018; Mahinzare et al. 2018; Gao et al. 2019). Many other works on the dynamics of nanobeams can be referred to the comprehensive review (Ebrahimi and Salari 2015; Ebrahimi and Barati 2018; Bouiadjra et al. 2013).

The buckling and post-buckling of graphene-reinforced laminated composite plates acted upon by uniaxial and biaxial forces were reported. The first order shear deformation theory was considered, and von Karman nonlinearity was employed to account for large deformation. Poly-methyl-methacrylate were used in the layers of the composite plate, and Halpin–Tsai and rule of mixtures were calibrated for the graphene composite, and graphene sheets were considered in perfect and defective forms. The incremental-iterative type of Ritz method was applied to solve the resulted stability equations. It was shown that the X-pattern has higher buckling loads for all types of boundary conditions (Karimi Zeverdejani et al. 2020). The forced vibration

and dynamic stability of thin rectangular microplates were investigated. The modified couple stress theory along with von Karman nonlinearity was utilized to obtain the kinematic relations, and Hamilton's principle was applied to obtain the governing partial differential equation of motion which was converted to a nonlinear ordinary differential equation using the Galerkin approach. The electrostatic pull-in voltages were determined, and the method of multiple scales was adopted to obtain the frequency curves for the primary, superharmonic, and subharmonic resonances (Karimipour et al. 2019). The buckling behavior of thin functionally graded Euler-Bernoulli beam in the frame work of the modified strain gradient theory was carried out. The differential equation for buckling with all possible boundary conditions is obtained using a variational statement. The influence of the power exponent parameter, the boundary conditions, scale parameter, beam thickness, and the slenderness ratio on the buckling behavior of the microbeams was discussed (Akgöz and Civalek 2013). Moreover, the bending, buckling, and vibration analysis of sinusoidal micro plates with simply supported boundary conditions were presented. The modified strain gradient theory was utilized, and the shear deformation was taken into consideration. Hamilton's principle was applied to derive the governing equations. Analytical solutions were obtained, and the effect of the scale parameter, the length-to-thickness ratio, and the shear deformation on the deflection, critical buckling loads, and the fundamental frequencies of the microplates (Akgöz and Civalek 2015).The bending response of porous functionally graded thick rectangular single-layer and sandwich plates according to a quasi 3D-shear deformation theory was studied. The governing equations were derived, and Navier's technique was presented to find the deflections and stresses for the FG simply supported plates (Zenkour 2011).

It is clear that mechanical behaviors of nanoplates are remarkably affected by temperature changes. As a result, the influence of thermal environments on the properties of buckling, transverse vibration, and bending of FG plates is one of the practical interesting subjects which has been investigated by many researchers (Barati and Shahverdi 2016; Ashoori et al. 2016; Ebrahimi and Barati 2016; Nami et al. 2015; Hong 2014; Shahsavari et al. 2018; Bouderba et al. 2013; Ebrahimi et al. 2016a; Goodarzi et al. 2016). Most recently, some researchers have studied mechanical behaviors of FG plates and nanoscale plates with considering thermal effects (Goodarzi et al. 2016; Hosseini et al. 2017; Kiani et al. 2018; Bakhsheshy and Khorshidi 2015; Bouderba et al. 2016; Bousahla et al. 2016; Karami et al. 2019; El-Haina et al. 2017; Barati and Shahverdi 2017; Khetir et al. 2017; Ashoori and Sadough Vanini 2016). Additionally, the buckling and vibration behaviors of FG nanoplates exposed to thermal environments have been a hot topic of research and interest in recent years (Sobhy 2015; Ghadiri et al. 2016; Sobhy and Radwan 2017) Furthermore, the static and vibrational characteristics of FG plates and nanoplates subjected to thermo-mechanical loads have been explored in the past years (Barati et al. 2016; Ebrahimi et al. 2016b; Saidi et al. 2013; Hosseini and Jamalpoor 2015).

To the authors' knowledge, studying the buckling behavior of FG nanoplates subjected to both biaxial mechanical forces and thermal effects has not been investigated. Therefore, the objective of this study is to fill the gap in developing a size-dependent model of a thin FG rectangular nanoplate subjected to biaxial linearly varying mechanical loads with various boundary conditions under three types of thermal loadings, namely uniform temperature rise, linear temperature change, and nonlinear temperature gradient thorough the thickness of the nanoplate. A brief overview of FG material, Eringen's nonlocal elasticity, and Kirchhoff's plate theory is given in the "Theoretical formulations of the FGM nanoplate under mechanical and thermal loads" section to derive the governing equation for the nanoplate. The "Chebyshev spectral collocation method for solving the governing equations of motion" section presents the Chebyshev spectral collocation method to obtain the numerical solutions. In the "Buckling characteristics of FG nanoplate under mechanical and thermal loadings" section, numerical results and parametric studies are given to report the critical thermal-mechanical buckling loads for a FG rectangular nonlocal nanoplate with different boundary conditions. The influence of the slope of the linearly varying forces, the aspect ratio, the nonlocal parameter, the different temperature rises, and the gradient index of the functionally graded material on the critical buckling loads are investigated and illustrated. In studying the effects of each of the mentioned parameters, the resulting nanoscale phenomena for the proposed system are

shown. Finally, concluding remarks are made in the "Conclusions" section.

Theoretical formulations of the FGM nanoplate under mechanical and thermal loads

Modeling of functionally graded nanoplates

A functionally graded rectangular nanoplate that is composed of ceramic and metal of length l, width b, and total thickness h is considered in this research, as shown in Fig. 1. The material properties of the FG nanoplate are assumed to vary continuously through the thickness of the nanoplate in accordance with a power law distribution as follows:

$$p(z) = p_{\mathrm{m}} + p_{\mathrm{cm}}\left(\frac{1}{2} + \frac{z}{h}\right)^{\mathrm{n}}; \qquad p_{\mathrm{cm}} = p_{\mathrm{c}} - p_{\mathrm{m}}; \qquad n \geq 0 \tag{1}$$

where $p(z)$ denotes the effective material property through the thickness of the nanoplate, such as Young's modulus E, thermal expansion coefficient α, and mass density ρ. The subscripts m and c represent the metallic and ceramic constituents, respectively. The thickness coordinate is represented by z and varies from $-h/2$ to $h/2$, and n refers to the volume fraction exponent. Since the effects of the variation of Poisson's ratio υ on the response of FG nanoplates are very small, it is assumed to be constant and is taken to be 0.3 through the analysis.

Overview of Eringen's nonlocal elasticity to account for size-dependent phenomena

The nonlocal elasticity theory, first introduced by Eringen (Eringen 2002), has been widely used to analyze nanoscale structures. As for physical interpretation, the nonlocal elasticity theory incorporates long range interactions between points in an elastic medium. According to this theory, the stress at a point is dependent on the strains of an extended region around that point in the body, as opposed to only the strain at the considered point. Thus, the stress tensor σ at a point x is defined as follows:

$$\sigma_{\mathrm{ij}}(x) = \iiint_V \varphi\left(|x' - x|, \mu\right) t_{\mathrm{ij}}\left(x'\right) \mathrm{d}V\left(x'\right) \tag{2}$$

where σ_{ij} and t_{ij} are the nonlocal and classical stress tensors, respectively; V is the volume of a region of the body that integral is taken on it, and $\varphi(|x'-x|\ \mu)$ denotes the nonlocal modulus, also referred to as the attenuation or kernel function which includes the nonlocal effects at a reference point x produced by the strains at x and x'. As it is seen from the above equation, the nonlocal modulus is dependent on two parameters, namely $|x'-x|$ and μ. $|x'-x|$ refers to the distance between points x and x', and μ represents the nonlocal parameter which is given by:

$$\mu = \frac{e_0 l_{\mathrm{i}}}{l} \tag{3}$$

where l_{i} and l denote the internal and external characteristic lengths, respectively, and e_0 is a constant that should be determined from the acoustic dispersions of the considered material.

As the integral form given in Eq. (2) is difficult to apply, Eringen (Eringen 1983) proposed an equivalent differential form of the nonlocal stress at any point x as follows:

$$\left(1 - (e_0 l_{\mathrm{i}})^2 \nabla^2\right) \sigma_{\mathrm{ij}} = t_{\mathrm{ij}} \tag{4}$$

where $e_0 l_{\mathrm{i}}$ denotes the nonlocal parameter, and $\nabla^2 = (\partial^2/\partial x^2) + (\partial^2/\partial y^2)$ is the two-dimensional Laplacian

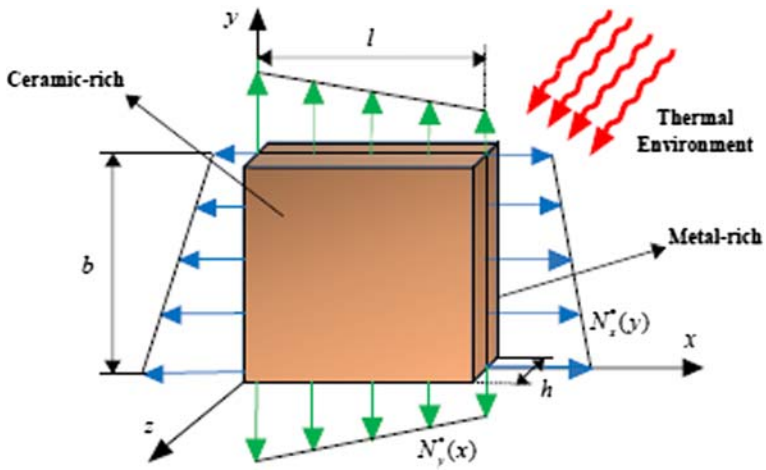

Fig. 1 Schematic configuration and the coordinate system of FGM rectangular nanoplate exposed to linearly varying biaxial mechanical loading and thermal environment

operator. It is obvious that the classical relationship between the stress and strain tensors can be obtained by setting the nonlocal parameter equal to zero in Eq. (4).

Displacement field for a FG nanoplate using Kirchhoff classical plate theory

The displacements of an arbitrary point of the FG nanoplate can be defined in Cartesian coordinates as follows:

$$u(x,y,z) = -z\frac{\partial w(x,y)}{\partial x}, \quad v(x,y,z) = -z\frac{\partial w(x,y)}{\partial y}, \quad w(x,y,z) = w(x,y) \tag{5}$$

where u, v, and w are the displacements in the x, y, and z directions, respectively. Using the displacements introduced in Eq. (5), the strain-displacement relations are given as functions of the transverse deflection w as:

$$\varepsilon_{xx} = -z\frac{\partial^2 w}{\partial x^2}, \quad \varepsilon_{yy} = -z\frac{\partial^2 w}{\partial y^2}, \quad \varepsilon_{xy} = -2z\frac{\partial^2 w}{\partial x \partial y} \tag{6}$$

Considered forms of thermal loads on the FG nanoplate

Uniform temperature distribution

In the case of uniform temperature distribution (UTD) across the thickness of the nanoplate, the temperature field can be expressed as:

$$T(z) = T_0 + \Delta T_0 \tag{7}$$

where T_0 is an arbitrary reference temperature at which no thermal strain is observed in the nanoplate, and ΔT_0 is the uniform temperature rise. It should be noted that for this case, *T(z)* is a constant and does not vary through the thickness of the plate, as in the case of the linear and nonlinear temperature distributions.

Linear temperature distribution

For a thin enough nanoplate, the temperature distribution is assumed to vary linearly along the thickness as follows (Kiani et al. 2011):

$$T(z) = T_m + (T_c - T_m)\left(\frac{1}{2} + \frac{z}{h}\right) \tag{8}$$

here, T_c and T_m represent the temperature of the ceramic-rich surface and metal-rich surface, respectively.

Nonlinear temperature distribution

In the case that the FG nanoplate is subjected to one-dimensional heat conduction in the z direction, the steady-state heat conduction equation absence of heat generation, and the boundary conditions are given as:

$$\frac{d}{dz}\left(k(z)\frac{dT}{dz}\right) = 0, \quad T(h/2) = T_c, \quad T(-h/2) = T_m \tag{9}$$

where *k(z)* denotes the effective thermal conductivity of the FG nanoplate and is given as:

$$k(z) = k_m + k_{cm}\left(\frac{1}{2} + \frac{z}{h}\right)^n, \quad k_{cm} = k_c - k_m \tag{10}$$

The above differential equation can be solved via the polynomial series. After applying the boundary conditions, the temperature field through the thickness of the nanoplate is expressed as (Javaheri and Eslami 2002):

$$T(z) = T_m + (T_c - T_m)\eta(z) \tag{11}$$

where

$$\eta(z) = \frac{1}{C}\left[\left(\frac{2z+h}{2h}\right) - \frac{k_{cm}}{(n+1)k_m}\left(\frac{2z+h}{2h}\right)^{n+1} + \frac{k_{cm}^2}{(2n+1)k_m^2}\left(\frac{2z+h}{2h}\right)^{2n+1} - \frac{k_{cm}^3}{(3n+1)k_m^3}\left(\frac{2z+h}{2h}\right)^{3n+1} + \frac{k_{cm}^4}{(4n+1)k_m^4}\left(\frac{2z+h}{2h}\right)^{4n+1} - \frac{k_{cm}^5}{(5n+1)k_m^5}\left(\frac{2z+h}{2h}\right)^{5n+1}\right] \tag{12}$$

and

$$C = 1 - \frac{k_{cm}}{(n+1)k_m} + \frac{k_{cm}^2}{(2n+1)k_m^2} - \frac{k_{cm}^3}{(3n+1)k_m^3} + \frac{k_{cm}^4}{(4n+1)k_m^4} - \frac{k_{cm}^5}{(5n+1)k_m^5} \tag{13}$$

It should be mentioned that, in the case of linear and nonlinear temperature gradients, the temperature difference can be expressed as:

$$\Delta T = T_c - T_m \tag{14}$$

Fundamental relations between mechanical and thermal strain: the thermos-elastic equations

For an elastic plate exposed to both mechanical and thermal stresses, the two-dimensional strain-stress relations at a point are expressed as (Jones 2006):

$$\varepsilon_{xx} = \frac{1}{E}\left(\sigma_{xx} - \nu\sigma_{yy}\right) + \alpha\Delta T_0 \tag{15}$$

$$\varepsilon_{yy} = \frac{1}{E}\left(\sigma_{yy} - \nu\sigma_{xx}\right) + \alpha\Delta T_0 \tag{16}$$

$$\varepsilon_{xy} = \frac{\sigma_{xy}}{G} \tag{17}$$

where ε_{xx} and ε_{yy} denote the total normal strains, and ε_{xy} represent the shear strain, while $\alpha\Delta T$ is representative of the thermal strain resulting from the temperature change at any point in the plate volume.

Governing equations of motion based on Kirchhoff's plate theory and Eringen's nonlocal theory

Considering Eringen's differential operator, Hooke's law, and thermal effects on the nanoplate, the constitutive relations between stresses and strains can be given by:

$$\sigma_{xx} - (e_0 a)^2\left(\frac{\partial^2\sigma_{xx}}{\partial x^2} + \frac{\partial^2\sigma_{xx}}{\partial y^2}\right) = \frac{E(z)}{1-\nu^2}\left[\varepsilon_{xx} + \nu\varepsilon_{yy} - \alpha(z)(T(z)-T_0)(1+\nu)\right] \tag{18}$$

$$\sigma_{yy} - (e_0 a)^2\left(\frac{\partial^2\sigma_{yy}}{\partial x^2} + \frac{\partial^2\sigma_{yy}}{\partial y^2}\right) = \frac{E(z)}{1-\nu^2}\left[\varepsilon_{yy} + \nu\varepsilon_{xx} - \alpha(z)(T(z)-T_0)(1+\nu)\right] \tag{19}$$

$$\sigma_{xy} - (e_0 a)^2\left(\frac{\partial^2\sigma_{xy}}{\partial x^2} + \frac{\partial^2\sigma_{xy}}{\partial y^2}\right) = G(z)\varepsilon_{xy} \tag{20}$$

where σ_{xx} and σ_{yy} denote the axial mechanical stresses in the x and y directions, respectively, and σ_{xy} refers to the shear stress. As previously mentioned, $T(z)$ is the temperature distribution along the thickness direction of the nanoplate, and T_0 is an arbitrary reference temperature; ν and $\alpha(z)$ are the Poisson's ratio and the thermal expansion coefficient of the nanoplate, respectively, $E(z)$ refers to the effective Young's modulus of the FG nanoplate, and $G(z)$ denotes the shear modulus which can be expressed in terms of the Young's modulus by the following equation:

$$G(z) = \frac{E(z)}{2(1+\nu)} \tag{21}$$

The resultant forces and moments are defined as:

$$\left\{N_x, N_y, N_{xy}\right\} = \int_{-h/2}^{h/2}\left\{\sigma_{xx}, \sigma_{yy}, \sigma_{xy}\right\} dz \tag{22}$$

and

$$\left\{M_x, M_y, M_{xy}\right\} = \int_{-h/2}^{h/2}\left\{\sigma_{xx}, \sigma_{yy}, \sigma_{xy}\right\} z\, dz \tag{23}$$

Substituting Eqs. (18–20) into Eqs. (22) and (23), the resultant forces and moments are derived as follows:

$$N_x - (e_0 a)^2\left(\frac{\partial^2 N_x}{\partial x^2} + \frac{\partial^2 N_x}{\partial y^2}\right) = -B_1\left(\frac{\partial^2 w}{\partial x^2} + \nu\frac{\partial^2 w}{\partial y^2}\right) - \frac{1}{1-\nu} \times \int_{-h/2}^{h/2} E(z)\alpha(z)(T(z)-T_0)dz \tag{24}$$

$$N_y - (e_0 a)^2\left(\frac{\partial^2 N_y}{\partial x^2} + \frac{\partial^2 N_y}{\partial y^2}\right) = -B_1\left(\frac{\partial^2 w}{\partial y^2} + \nu\frac{\partial^2 w}{\partial x^2}\right) - \frac{1}{1-\nu} \times \int_{-h/2}^{h/2} E(z)\alpha(z)(T(z)-T_0)dz \tag{25}$$

$$N_{xy} - (e_0 a)^2\left(\frac{\partial^2 N_{xy}}{\partial x^2} + \frac{\partial^2 N_{xy}}{\partial y^2}\right) = -B_2\left(\frac{\partial^2 w}{\partial x \partial y}\right) \tag{26}$$

$$M_x - (e_0 a)^2 \left(\frac{\partial^2 M_x}{\partial x^2} + \frac{\partial^2 M_x}{\partial y^2} \right) = -D_1 \left(\frac{\partial^2 w}{\partial x^2} + \nu \frac{\partial^2 w}{\partial y^2} \right) - \left(\frac{1}{1-\nu} \right) \int_{-h/2}^{h/2} E(z)\alpha(z)(T(z)-T_0) z dz \quad (27)$$

$$M_y - (e_0 a)^2 \left(\frac{\partial^2 M_y}{\partial x^2} + \frac{\partial^2 M_y}{\partial y^2} \right) = -D_1 \left(\frac{\partial^2 w}{\partial y^2} + \nu \frac{\partial^2 w}{\partial x^2} \right) - \left(\frac{1}{1-\nu} \right) \int_{-h/2}^{h/2} E(z)\alpha(z)(T(z)-T_0) z dz \quad (28)$$

$$M_{xy} - (e_0 a)^2 \left(\frac{\partial^2 M_{xy}}{\partial x^2} + \frac{\partial^2 M_{xy}}{\partial y^2} \right) = -D_2 \left(\frac{\partial^2 w}{\partial x \partial y} \right) \quad (29)$$

where

$$(B_1, D_1) = \int_{-h/2}^{h/2} \frac{E(z)(z, z^2) dz}{1-\nu^2} \quad (30)$$

and

$$(B_2, D_2) = \int_{-h/2}^{h/2} \frac{E(z)(z, z^2) dz}{2(1+\nu)} \quad (31)$$

The axial forces in the x and y directions are given by:

$$N_x = N_x^M + N^T \quad (32)$$

$$N_y = N_y^M + N^T \quad (33)$$

In this study, N_x^M and N_y^M are linearly varying mechanical loads exerted on the FG nanoplate in the x and y directions, respectively, and N^T is the thermal resultant which can be defined as:

$$N_x^M = \zeta_1 P\left(1-\gamma_1 \frac{y}{b}\right), \quad N_y^M = \zeta_2 P\left(1-\gamma_2 \frac{x}{l}\right) \quad (34)$$

$$N^T = -\left(\frac{1}{1-\nu} \right) \int_{-h/2}^{h/2} E(z)\alpha(z)(T(z)-T_0)\, dz \quad (35)$$

where P denotes the axial load at the origin of the Cartesian coordinate system defined on the rectangular nanoplate. The slopes of the linear mechanical loads are denoted by factors γ_1 and γ_2. ζ_1 and ζ_2 represent the load parameters, such that in the case of the biaxial compression in the x and y directions, $\zeta_1 = \zeta_2 = -1$.

Using the minimum total potential energy principle, the equilibrium equation of an initially preloaded rectangular plate subjected to thermal loads is obtained as follow:

$$\frac{\partial^2 M_x}{\partial x^2} + \frac{\partial^2 M_y}{\partial y^2} + 2\frac{\partial^2 M_{xy}}{\partial x \partial y} + \left(N_x^M + N^T\right)\frac{\partial^2 w}{\partial x^2} + \left(N_y^M + N^T\right)\frac{\partial^2 w}{\partial y^2} + 2N_{xy}\frac{\partial^2 w}{\partial x \partial y} = 0 \quad (36)$$

The second derivatives of Eq. (36) with respect to x and y are derived as:

$$\frac{\partial^4 M_x}{\partial x^4} + \frac{\partial^4 M_y}{\partial x^2 \partial y^2} + 2\frac{\partial^4 M_{xy}}{\partial x^3 \partial y} + \frac{\partial^2}{\partial x^2}\left(\left(N_x^M + N^T\right)\frac{\partial^2 w}{\partial x^2}\right) + \frac{\partial^2}{\partial x^2}\left(\left(N_y^M + N^T\right)\frac{\partial^2 w}{\partial y^2}\right) + \frac{\partial^2}{\partial x^2}\left(2N_{xy}\frac{\partial^2 w}{\partial x \partial y}\right) = 0 \quad (37)$$

$$\frac{\partial^4 M_x}{\partial x^2 \partial y^2} + \frac{\partial^4 M_y}{\partial y^4} + 2\frac{\partial^4 M_{xy}}{\partial x \partial y^3} + \frac{\partial^2}{\partial y^2}\left(\left(N_x^M + N^T\right)\frac{\partial^2 w}{\partial x^2}\right) + \frac{\partial^2}{\partial y^2}\left(\left(N_y^M + N^T\right)\frac{\partial^2 w}{\partial y^2}\right) + \frac{\partial^2}{\partial y^2}\left(2N_{xy}\frac{\partial^2 w}{\partial x \partial y}\right) = 0 \quad (38)$$

The second derivative of Eq. (27) with respect to x, the second derivative of Eq. (28) with respect to y, and the partial derivative of Eq. (29) with respect to x then with respect to y can be given by:

$$\frac{\partial^2 M_x}{\partial x^2} = (e_0 a)^2 \left(\frac{\partial^4 M_x}{\partial x^4} + \frac{\partial^4 M_x}{\partial x^2 \partial y^2} \right) - D\left(\frac{\partial^4 w}{\partial x^4} + \nu \frac{\partial^4 w}{\partial x^2 \partial y^2} \right) \quad (39)$$

$$\frac{\partial^2 M_y}{\partial y^2} = (e_0 a)^2 \left(\frac{\partial^4 M_y}{\partial x^2 \partial y^2} + \frac{\partial^4 M_y}{\partial y^4} \right) - D\left(\frac{\partial^4 w}{\partial y^4} + \nu \frac{\partial^4 w}{\partial x^2 \partial y^2} \right) \quad (40)$$

$$\frac{\partial^2 M_{xy}}{\partial x \partial y} = (e_0 a)^2 \left(\frac{\partial^4 M_{xy}}{\partial x^3 \partial y^2} + \frac{\partial^4 M_{xy}}{\partial x \partial y^3} \right) - D(1-\nu)\left(\frac{\partial^4 w}{\partial x^2 \partial y^2} \right) \quad (41)$$

here, D is the flexural rigidity of the functionally graded nanoplate and it can be introduced as:

$$D = D_1 - \frac{B_1^2}{A_1} \tag{42}$$

and

$$(A_1, B_1, D_1) = \int_{-h/2}^{h/2} \frac{E(z)(1, z, z^2)}{1-\nu^2}\, dz \tag{43}$$

Summing Eqs. (37) and (38), we obtain:

$$\frac{\partial^4 M_x}{\partial x^4} + \frac{\partial^4 M_y}{\partial x^2 \partial y^2} + 2\frac{\partial^4 M_{xy}}{\partial x^3 \partial y} + \frac{\partial^4 M_x}{\partial x^2 \partial y^2} + \frac{\partial^4 M_y}{\partial y^4} + 2\frac{\partial^4 M_{xy}}{\partial x \partial y^3} = -\left(\frac{\partial^2}{\partial x^2} + \frac{\partial^2}{\partial y^2}\right)\left(\left(N_x^M + N^T\right)\frac{\partial^2 w}{\partial x^2} + \left(N_y^M + N^T\right)\frac{\partial^2 w}{\partial y^2} + 2N_{xy}\frac{\partial^2 w}{\partial x \partial y}\right) \tag{44}$$

Summing Eqs. (39), (40), and twice of Eq. (41), inserting them into Eq. (36) and using the Eq. (44), yield the following equation as:

$$D\left(\frac{\partial^4 w}{\partial x^4} + \frac{\partial^4 w}{\partial y^4} + 2\frac{\partial^4 w}{\partial x^2 \partial y^2}\right) - N^T\left(\frac{\partial^2 w}{\partial x^2} + \frac{\partial^2 w}{\partial y^2}\right) + N^T(e_0 a)^2\left(\frac{\partial^4 w}{\partial x^4} + 2\frac{\partial^4 w}{\partial x^2 \partial y^2} + \frac{\partial^4 w}{\partial y^4}\right) = \left(1-(e_0 a)^2\left(\frac{\partial^2}{\partial x^2} + \frac{\partial^2}{\partial y^2}\right)\right)\left(N_x^M \frac{\partial^2 w}{\partial x^2} + N_y^M \frac{\partial^2 w}{\partial y^2} + 2N_{xy}\frac{\partial^2 w}{\partial x \partial y}\right) \tag{45}$$

Substituting Eq. (34) into Eq. (45) and setting $N_{xy} = 0$ yield:

$$D\left(\frac{\partial^4 w}{\partial x^4} + \frac{\partial^4 w}{\partial y^4} + 2\frac{\partial^4 w}{\partial x^2 \partial y^2}\right) - N^T\left(\frac{\partial^2 w}{\partial x^2} + \frac{\partial^2 w}{\partial y^2}\right) + N^T(e_0 a)^2\left(\frac{\partial^4 w}{\partial x^4} + 2\frac{\partial^4 w}{\partial x^2 \partial y^2} + \frac{\partial^4 w}{\partial y^4}\right) = \left(1-(e_0 a)^2\left(\frac{\partial^2}{\partial x^2} + \frac{\partial^2}{\partial y^2}\right)\right)\left(\zeta_1 P\left(1-\gamma_1 \frac{y}{b}\right)\frac{\partial^2 w}{\partial x^2} + \zeta_2 P\left(1-\gamma_2 \frac{x}{l}\right)\frac{\partial^2 w}{\partial y^2}\right) \tag{46}$$

Expanding the derivatives in Eq. (46) gives the governing equation in terms of the transverse deflection of the nanoplate as follows:

$$D\left(\frac{\partial^4 w}{\partial x^4} + \frac{\partial^4 w}{\partial y^4} + 2\frac{\partial^4 w}{\partial x^2 \partial y^2}\right) - N^T\left(\frac{\partial^2 w}{\partial x^2} + \frac{\partial^2 w}{\partial y^2}\right) + N^T(e_0 a)^2 \left(\frac{\partial^4 w}{\partial x^4} + 2\frac{\partial^4 w}{\partial x^2 \partial y^2} + \frac{\partial^4 w}{\partial y^4}\right) = \zeta_1 P\left(1-\gamma_1 \frac{y}{b}\right)\frac{\partial^2 w}{\partial x^2} + 2\zeta_1 P(e_0 a)^2 \left(\frac{\gamma_1}{b}\right)\frac{\partial^3 w}{\partial x^2 \partial y} - \zeta_1 P(e_0 a)^2\left(1-\gamma_1 \frac{y}{b}\right)\frac{\partial^4 w}{\partial x^2 \partial y^2} - \zeta_1 P(e_0 a)^2\left(1-\gamma_1 \frac{y}{b}\right)\frac{\partial^4 w}{\partial x^4} + \zeta_2 P\left(1-\gamma_2 \frac{x}{l}\right)\frac{\partial^2 w}{\partial y^2} + 2\zeta_2 P(e_0 a)^2\left(\frac{\gamma_2}{l}\right)\frac{\partial^3 w}{\partial x \partial y^2} - \zeta_2 N_0 (e_0 a)^2 \left(1-\gamma_2 \frac{x}{l}\right)\frac{\partial^4 w}{\partial x^2 \partial y^2} - \zeta_2 N_0 (e_0 a)^2\left(1-\gamma_2 \frac{x}{l}\right)\frac{\partial^4 w}{\partial y^4} \tag{47}$$

The dimensionless parameters are defined below to derive the normalized governing equation.

$$T_n = \frac{l^2 N^T}{D}, \quad W = \frac{w}{l}, \quad X = \frac{x}{l}, \quad Y = \frac{y}{b}, \quad \lambda = \frac{l}{b}, \quad \mu = \frac{e_0 a}{l}, \quad N^* = \frac{P l^2}{D} \tag{48}$$

Substituting the dimensionless parameters given in Eq. (48) into Eq. (47), the normalized governing equation for a rectangular nanoplate subjected to biaxial mechanical loads in high temperature environments with considering thermal loads can be derived as:

$$\left(\frac{\partial^4 W}{\partial X^4} + 2\lambda^2 \frac{\partial^4 W}{\partial X^2 \partial Y^2} + \lambda^4 \frac{\partial^4 W}{\partial Y^4}\right) - T_n\left(\frac{\partial^2 W}{\partial X^2} + \lambda^2 \frac{\partial^2 W}{\partial Y^2}\right) + T_n \mu^2 \left(\frac{\partial^4 W}{\partial X^4} + 2\lambda^2 \frac{\partial^4 W}{\partial X^2 \partial Y^2} + \lambda^4 \frac{\partial^4 W}{\partial Y^4}\right) = \zeta_1 N^*(1-\gamma_1 Y)\frac{\partial^2 W}{\partial X^2} + 2\zeta_1 N^* \mu^2 \gamma_1 \lambda^2 \frac{\partial^3 W}{\partial X^2 \partial Y} - \zeta_1 N^* \mu^2 \lambda^2 (1-\gamma_1 Y)\frac{\partial^4 W}{\partial X^2 \partial Y^2} - \zeta_1 N^* \mu^2 (1-\gamma_1 Y)\frac{\partial^4 W}{\partial X^4} + \zeta_2 N^* \lambda^2 (1-\gamma_2 X)\frac{\partial^2 W}{\partial Y^2} + 2\zeta_2 N^* \mu^2 \gamma_2 \lambda^2 \frac{\partial^3 W}{\partial X \partial Y^2} - \zeta_2 N^* \mu^2 \lambda^2 (1-\gamma_2 X)\frac{\partial^4 W}{\partial X^2 \partial Y^2} - \zeta_2 N^* \mu^2 \lambda^4 (1-\gamma_2 X)\frac{\partial^4 W}{\partial Y^4} \tag{49}$$

Chebyshev spectral collocation method for solving the governing equations of motion

The Chebyshev spectral collocation method, which has high accuracy and a fast rate of convergence (compared with other powerful numerical techniques), is used for the spatial discretization of the governing equation of motion and boundary conditions. Chebyshev nodes are the roots of the Chebyshev polynomials of the first kind and are the projections of equally spaced segments of a unit circle on the interval [− 1, − 1] and are defined as:

$$x_j = \cos(j\pi/N), \quad j = 0, 1, \ldots, N \tag{50}$$

The Chebyshev differentiation matrix, $[D]_N$, is extracted by interpolating a Lagrange polynomial of degree N at each Chebyshev point, differentiating the polynomial, and finding its derivative at each point. This matrix has a size of $(N + 1) \times (N + 1)$, and its elements are given as:

$$\begin{aligned}
&(D_N)_{00} = \frac{2N^2+1}{6}, \quad (D_N)_{00} = -\frac{2N^2+1}{6}\\
&(D_N)_{jj} = \frac{-x_j}{2\left(1-x_j^2\right)}, \quad j = 1, \ldots, N-1\\
&(D_N)_{ij} = \frac{c_i}{c_j}\frac{(-1)^{i+j}}{(x_i-x_j)}, \quad i \neq j, \quad i, j = 0, \ldots, N\\
&c_i = \begin{cases} 2, & i = 0 \text{ or } N \\ 1, & \text{otherwise} \end{cases}
\end{aligned} \tag{51}$$

Based on the Chebyshev spectral collocation method, the n^{th} derivative of a general function can be expressed as:

$$Dn = (D_N)^n \tag{52}$$

Making use of the Chebyshev method and the Kronecker product, the governing equations and boundary conditions are discretized in the space domain. Subsequently, the displacement vector of the nanoplate can be given by:

$$[U]^T = \left[W_{(1,1)}, W_{(1,2)}, \ldots, W_{(M,M)}\right], \quad M = N + 1 \tag{53}$$

here, M refers to the number of points in the x and y directions. Employing the spatial discretization procedure, the left-hand side of Eq. (49) can be rewritten as:

$$\begin{aligned}
LH = &\left(1 + T_n\mu^2\right)\left[(D4\otimes I) + 2\lambda^2(D2\otimes D2) + \lambda^4(I\otimes D4)\right]\\
&-T_n\left[(D2\otimes I) + \lambda^2(I\otimes D2)\right]
\end{aligned} \tag{54}$$

in which I represents an $M \times M$ identity matrix. Similarly, the right-hand side of Eq. (49) is discretized as follows:

$$\begin{aligned}
N^* \times (RH) = N^*\big[&\zeta_1(D2\otimes H(Y)) + 2\zeta_1\gamma_1\lambda^2\mu^2(D2\otimes D1) - \zeta_1\lambda^2\mu^2(D2\otimes H(Y)*D2)\\
&-\zeta_1\mu^2(D4\otimes H(Y)) + \zeta_2\lambda^2(G(X)\otimes D2) + 2\zeta_2\gamma_2\lambda^2\mu^2(D1\otimes D2)\\
&-\zeta_2\lambda^2\mu^2(D2\otimes G(X)*D2) - \zeta_2\lambda^4\mu^2(G(X)\otimes D4)\big]
\end{aligned} \tag{55}$$

and

$$G(X) = 1-\gamma_2 X, \qquad H(Y) = 1-\gamma_1 Y \tag{56}$$

Consequently, the discretized form of the governing equation of the nanoplate can be expressed as:

$$[LH]\{W\} = N^*[RH]\{W\} \tag{57}$$

In the equations above, the normalized X and Y axes are in the range of [0, 1].

In the present article, two boundary conditions are considered: simply supported and clamped. Mathematically, they are expressed as:

(i) Clamped (C):

$$\begin{aligned}
&W(0, Y) = 0, \quad \partial W(0, Y)/\partial X = 0\\
&W(1, Y) = 0, \quad \partial W(1, Y)/\partial X = 0\\
&W(X, 0) = 0, \quad \partial W(X, 0)/\partial Y = 0\\
&W(X, 1) = 0, \quad \partial W(X, 1)/\partial Y = 0
\end{aligned} \tag{58}$$

(ii) Simply supported (S):

$$\begin{aligned}
&W(0, Y) = 0, \quad \partial^2 W(0, Y)/\partial X^2 = 0\\
&W(1, Y) = 0, \quad \partial^2 W(1, Y)/\partial X^2 = 0\\
&W(X, 0) = 0, \quad \partial^2 W(X, 0)/\partial Y^2 = 0\\
&W(X, 1) = 0, \quad \partial^2 W(X, 1)/\partial Y^2 = 0
\end{aligned} \tag{59}$$

These boundary conditions at the four edges of the FG nanoplate are discretized by adopting the Chebyshev's approach and the Kronecker product, as mentioned below:

Clamped (C) at $X = 0$:

$$\begin{aligned}
&([1, 0, \ldots, 0]\otimes I)\left\{W^T\right\}\\
&= 0, \quad (D1(1, :)\otimes I)\left\{W^T\right\} = 0
\end{aligned} \tag{60}$$

where the vector $D1(1, :)$is defined as:

$$D1(1, :) = \left[D1(1, 1), D1\left(1, 2\right), \ldots, D1\left(1, M-1\right), D1\left(1, M\right)\right] \tag{61}$$

Clamped (C) at $X = 1$:

$$\begin{aligned}
&([0, 0, \ldots, 1]\otimes I)\left\{W^T\right\}\\
&= 0, \quad (D1(M, :)\otimes I)\left\{W^T\right\} = 0
\end{aligned} \tag{62}$$

and

$$D1(M,:) = \left[D1(M,1), D1\left(M,2\right), ..., D1\left(M,M-1\right), D1\left(M,M\right)\right] \tag{63}$$

Simply supported (S) at $X = 0$:

$$\left([1,0,...,0]\otimes I\right)\left\{W^{\mathrm{T}}\right\} = 0, \quad \left(D2(1,:)\otimes I\right)\left\{W^{\mathrm{T}}\right\} = 0 \tag{64}$$

in which

$$D2(1,:) = \left[D2(1,1), D2\left(1,2\right), ..., D2\left(1,M-1\right), D2\left(1,M\right)\right] \tag{65}$$

Simply supported (S) at $X = 1$:

$$\left([0,0,...,1]\otimes I\right)\left\{W^{\mathrm{T}}\right\} = 0, \quad \left(D2(M,:)\otimes I\right)\left\{W^{\mathrm{T}}\right\} = 0 \tag{66}$$

here, the vector $D2(M, :)$ can be written as:

$$D2(M,:) = \left[D2(M,1), D2\left(M,2\right), ..., D2\left(M,M-1\right), D2\left(M,M\right)\right] \tag{67}$$

Clamped (C) at $Y = 0$:

$$\left(I\otimes[1,0,...,0]\right)\left\{W^{\mathrm{T}}\right\} = 0, \quad \left(I\otimes D1(1,:)\right)\left\{W^{\mathrm{T}}\right\} = 0 \tag{68}$$

Clamped (C) at $Y = 1$:

$$\left(I\otimes[0,0,...,1]\right)\left\{W^{\mathrm{T}}\right\} = 0, \quad \left(I\otimes D1(M,:)\right)\left\{W^{\mathrm{T}}\right\} = 0 \tag{69}$$

Simply supported (S) at $Y = 0$:

$$\left(I\otimes[1,0,...,0]\right)\left\{W^{\mathrm{T}}\right\} = 0, \quad \left(I\otimes D2(1,:)\right)\left\{W^{\mathrm{T}}\right\} = 0 \tag{70}$$

Simply supported (S) at $Y = 1$:

$$\left(I\otimes[0,0,...,1]\right)\left\{W^{\mathrm{T}}\right\} = 0, \quad \left(I\otimes D2(M,:)\right)\left\{W^{\mathrm{T}}\right\} = 0 \tag{71}$$

Consequently, the discretized governing equations of the nanostructure can be given by:

$$\begin{bmatrix}[S_{\mathrm{BB}}] & [S_{\mathrm{BI}}]\\ [S_{\mathrm{IB}}] & [S_{\mathrm{II}}]\end{bmatrix}\begin{Bmatrix}\{W_{\mathrm{B}}\}\\ \{W_{\mathrm{I}}\}\end{Bmatrix} = N^{*}\begin{bmatrix}[0] & [0]\\ [0] & [Q]\end{bmatrix}\begin{Bmatrix}\{W_{\mathrm{B}}\}\\ \{W_{\mathrm{I}}\}\end{Bmatrix} \tag{72}$$

where W_{B} and W_{I} denote the displacement vectors at the boundaries and the interior points, respectively. In Eq. (72), S_{BB}, S_{BI}, S_{IB}, and S_{II} are matrices with sizes of $(8N - 16) \times (8N - 16)$, $(8N - 16) \times (N^2 - 8N + 16)$, $(N^2 - 8N + 16) \times (8N - 16)$, and $(N^2 - 8N + 16) \times (N^2 - 8N + 16)$, respectively.

Manipulating Eq. (72) yields the following formulations:

$$[S_{\mathrm{BB}}]\{W_{\mathrm{B}}\} + [S_{\mathrm{BI}}]\{W_{\mathrm{I}}\} = [0] \tag{73}$$

$$[S_{\mathrm{IB}}]\{W_{\mathrm{B}}\} + [S_{\mathrm{II}}]\{W_{\mathrm{I}}\} = N^{*}[Q]\{W_{\mathrm{I}}\} \tag{74}$$

Solving Eq. (73) for $\{W_{\mathrm{B}}\}$ gives the following equation:

$$\{W_{\mathrm{B}}\} = -[S_{\mathrm{BB}}]^{-1}[S_{\mathrm{BI}}]\{W_{\mathrm{I}}\} \tag{75}$$

By substituting Eq. (75) into Eq. (74), the equation used for eigenvalue problem analysis can be obtained as follows:

$$\left(-[S_{\mathrm{IB}}][S_{\mathrm{BB}}]^{-1}[S_{\mathrm{BI}}] + [S_{\mathrm{II}}]\right)\{W_{\mathrm{I}}\} = N^{*}[Q]\{W_{\mathrm{I}}\} \tag{76}$$

The previous equation can be rewritten as:

$$[Q]^{-1}\left(-[S_{\mathrm{IB}}][S_{\mathrm{BB}}]^{-1}[S_{\mathrm{BI}}] + [S_{\mathrm{II}}]\right)\{W_{\mathrm{I}}\} = N^{*}\{W_{\mathrm{I}}\} \tag{77}$$

and

$$A = [Q]^{-1}\left(-[S_{\mathrm{IB}}][S_{\mathrm{BB}}]^{-1}[S_{\mathrm{BI}}] + [S_{\mathrm{II}}]\right) \tag{78}$$

Performing an eigenvalue problem analysis and calculating the lowest eigenvalue of matrix A introduced in Eq. (78), we obtain the first critical buckling load of the rectangular FG nanoplate.

Buckling characteristics of FG nanoplate under mechanical and thermal loadings

In this section, the role and impact of different temperature gradients on the buckling characteristics of FG rectangular nanoplate based on the nonlocal elasticity theory and Kirchhoff's plate theory are demonstrated. A thin rectangular nanoplate with gradually varying composition, subjected to various thermal and bi-axial mechanical loads, is considered for the analyses. Numerical results are provided to indicate the influences of several parameters including temperature rise, nonlocality, gradient index, slopes of linearly varying mechanical forces, ratio of length to width, and various boundary conditions on the buckling response of a rectangular FG nanoplate with various temperature distributions.

Table 1 Mechanical and thermal properties of the materials of the FG nanoplate (Kiani et al. 2011)

Material	Young's modulus *(E)*	Poisson's ratio *(ν)*	Thermal expansion coefficient *(α)*	Thermal conductivity coefficient *(K)*
Metal	70 *GPa*	0.3	$23 \times 10^{-6}/C^0$	204 W/mC^0
Ceramic	380 *GPa*	0.3	$7.4 \times 10^{-6}/C^0$	10.4 W/mC^0

Moreover, the mechanical buckling load and the critical temperature are calculated for different types of temperature gradients including uniform, linear, and nonlinear temperature distributions through the thickness of the FG nanoplate. To illustrate the proposed model, a combination of a metal and a ceramic is considered, and their properties are tabulated in Table 1.

For the sake of brevity, a four-letter symbol is used to represent the various boundary conditions for the following four edges of the rectangular nanoplate, as shown in Fig. 2.

To show the accuracy of the proposed approach, comparative studies on the critical buckling temperature of the FG nanoplate are carried out in Tables 2 and 3 between the present results and those reported by Javaheri and Eslami (Javaheri and Eslami 2002). It can be noted that the results are in excellent agreement.

The treated two verification examples reveal that present approach can accurately predict the critical thermal buckling load for FG nanoplates under thermal loadings.

Impacts of temperature rise on the buckling characteristics of the FG nanoplate subjected to uniform temperature distribution

The effects of the temperature rise and the nonlocal parameter on the critical mechanical buckling load of the FG SSSS nanoplate ($h = 0.34$ nm, $n = 1$, $\lambda = 1$, $\zeta_1 = -1$, $\zeta_2 = -1$, $\gamma_1 = 0.1$, $\gamma_2 = 0.1$) subjected to biaxial compressive mechanical forces are examined in Fig. 3. It is observed that by increasing the temperature, the critical mechanical load needed to buckle the FG nanoplate would decrease seriously. This behavior is

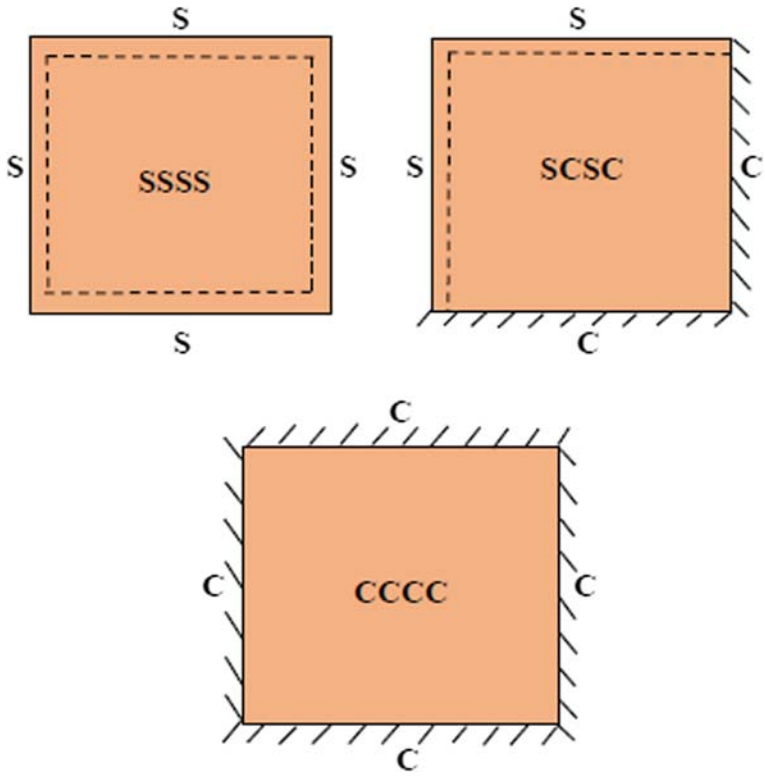

Fig. 2 Boundary conditions. S, simply supported; C, clamped

Table 2 Comparison of the critical buckling temperature difference for linear temperature distribution through the thickness of the SSSS FG nanoplate ($h/b = 0.01$)

n	Reference	$l/b = 1$	$l/b = 2$	$l/b = 3$	$l/b = 4$	$l/b = 5$
1	Present study	5.5209	27.8683	65.1139	117.2580	184.3000
	Javaheri and Eslami 2002	5.5209	27.8683	65.1140	117.2580	184.3003
5	Present study	3.8999	22.6597	53.9259	97.6985	153.9780
	Javaheri and Eslami 2002	3.8999	22.6595	53.9256	97.6981	153.9770

attributed to the softening effect of the temperature rise. Before buckling occurs, increasing the temperature of the nanoplate decreases its overall rigidity, and thus, the critical mechanical buckling load decreases drastically. It is also found that an increase in the value of the nonlocal parameter leads to the reduction of the critical mechanical buckling force, as predicted by Eringen's nonlocal elasticity theory for the prescribed boundary conditions. This is due to the fact that augmenting the nonlocality nature reduces the stiffness of the FG nanoplate.

In Fig. 4, the critical mechanical buckling load of the simply supported FG nanoplate exposed to linearly varying biaxial mechanical forces and uniform temperature gradient versus the temperature elevation for three different values of the aspect ratio, and the power law index is determined. As expected, it is clear that the buckling load generally decreases by the increase of the temperature due to the softening effect of temperature rise. Also, it can be seen from Fig. 4 that the critical buckling loads improve when the aspect ratio increases. While this may seem counterintuitive, it should be mentioned that in varying the aspect ratio of l/b, the ratio of h/l is kept constant. Due to the second ratio remaining constant for the analyses in Fig. 4, if the parameter l is increased through increasing the aspect ratio, the value of h also increases. Also, it should be noted that in Fig. 4, the dimensional results are presented. Referring to Eq. (49), which was used to nondimensionalize the equations of motion, the axial load was presented in the form $N^* = Pl^2/D$. Thus, for the same N^* and increasing l, P increases, as shown in the figure.

The influence of the power law index on the critical mechanical force to buckle the FG nanoplate is opposite to that of the aspect ratio. This is predictable because an increase of the power law index makes the FG nanoplate less stiff, i.e., contains a greater amount of the metal than the ceramic, and hence, lower critical buckling loads result. Here, it is inferred that for all values of the aspect ratio, the lower values of the power law index have more significant influence on the reduction of the mechanical buckling load, while increasing the power law index has no sensible effect on the buckling behavior of the FG nanoplate.

To determine the impacts of the nonlocal parameter, the aspect ratio, and the power law index on the critical temperature rise of the FG nanoplate, the critical buckling temperature elevations against the nonlocality index are plotted in Fig. 5 for three different values of aspect ratio and power law index, under uniform temperature distribution across the thickness of the SSSS FG nanoplate. As predicted, it is observable that the nonlocal parameter and the power law index exhibit reducing effects on the critical temperature rise by possessing softening influence on the FG nanoplate structure. As can be seen, for all cases, when the nonlocal parameter of the FG nanoplate increases up to 0.2, a swift decrease

Table 3 Comparison of the critical buckling temperature difference for nonlinear temperature distribution through the thickness of the SSSS FG nanoplate ($h/b = 0.01$)

n	Reference	$l/b = 1$	$l/b = 2$	$l/b = 3$	$l/b = 4$	$l/b = 5$
1	Present study	7.6636	38.6840	90.3847	162.7656	255.8268
	Javaheri and Eslami 2002	7.6635	38.6838	90.3842	162.7649	255.8257
5	Present study	4.8775	28.3391	67.4418	122.1854	192.5703
	Javaheri and Eslami 2002	4.8774	28.3389	67.4414	122.1849	192.5694

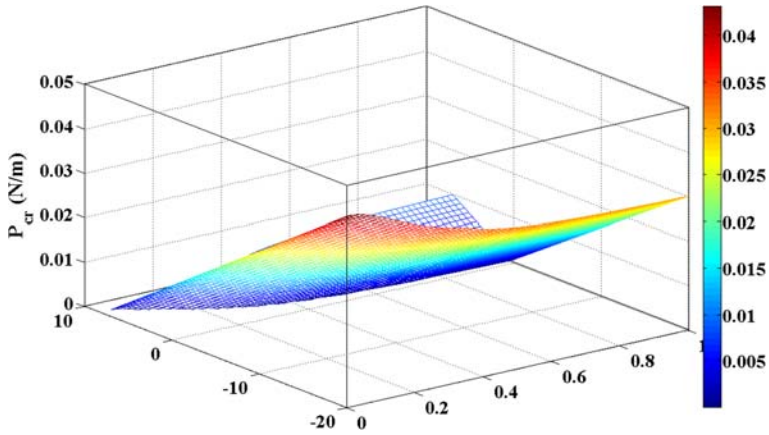

Fig. 3 Variation of the critical mechanical buckling load versus the temperature and nonlocal parameter for a thin SSSS functionally graded nanoplate subjected to bi-axial compressive loads and uniform temperature distribution (UTD), $h = 0.34$ nm, $n = 1$, $\lambda = 1$, $\zeta_1 = -1$, $\zeta_2 = -1$, $\gamma_1 = 0.1$, and $\gamma_2 = 0.1$

in the critical temperature rise occurs, and the rest of the curve is purely downward. In addition, as the FG nanoplate becomes softer, the effects of the power law index would diminish more. Furthermore, it can be concluded that an increase in the aspect ratio is accompanied by improving the critical temperature rise to buckle the system. Also, it is understood that by advancing the softening property of the nonlocality nature, the impact of the aspect ratio could manifest itself less.

In Fig. 6, the dependency of the critical mechanical buckling load of the FG nanoplate to the nonlocal parameter and the slope of change in the mechanical force exerted on the nanoplate in the x direction, when the SSSS FG nanoplate is subjected to uniform temperature distribution across the thickness, is shown. As explained earlier, it is apparent that by increasing the nonlocal parameter, the critical mechanical load would decrease due to the softening behavior of the nonlocality nature. From Fig. 6, it is clear that augmenting the slope of the linearly varying mechanical load in the x direction causes an increase in the mechanical force required to buckle the nanoplate for a fixed value of the slope of load variation in the y direction. This is predicted because increasing the slope of the load reduces the average value of the mechanical load applied on the FG nanoplate axially, and hence, the value of the critical mechanical load would increase. This can easily be seen by referring to Eq. (35), in which it is shown that the

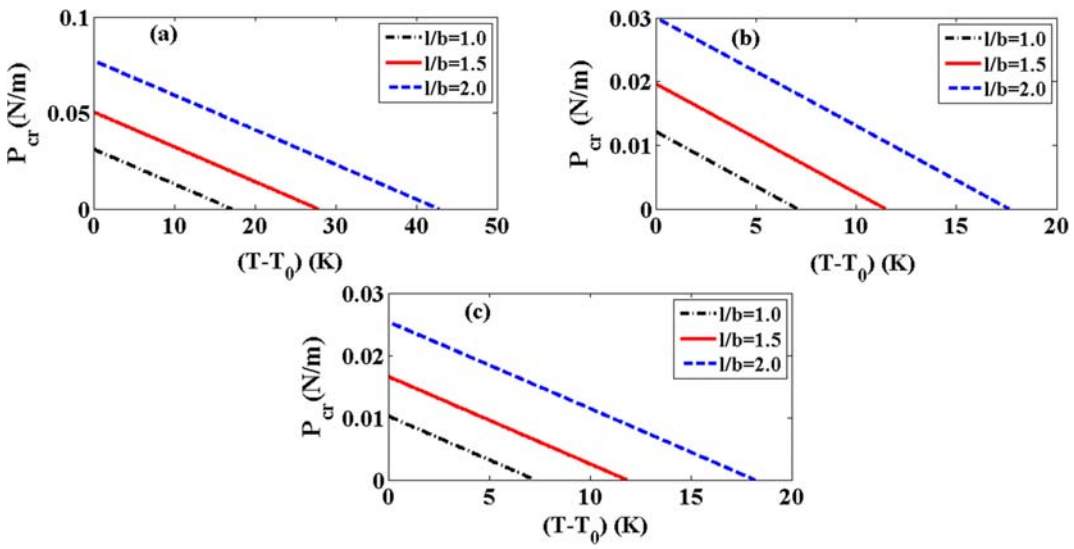

Fig. 4 Variation of the critical mechanical buckling load with respect to the temperature rise for a thin SSSS functionally graded nanoplate subjected to bi-axial compressive loads under uniform temperature distribution (UTD) for different values of aspect ratio and power law index, $h/l = 0.01$, $\zeta_1 = -1$, $\zeta_2 = -1$, $\gamma_1 = 0.5$, $\gamma_2 = 0.5$,$\mu = 0$. **a** $n = 0$. **b** $n = 2$.**c** $n = 5$

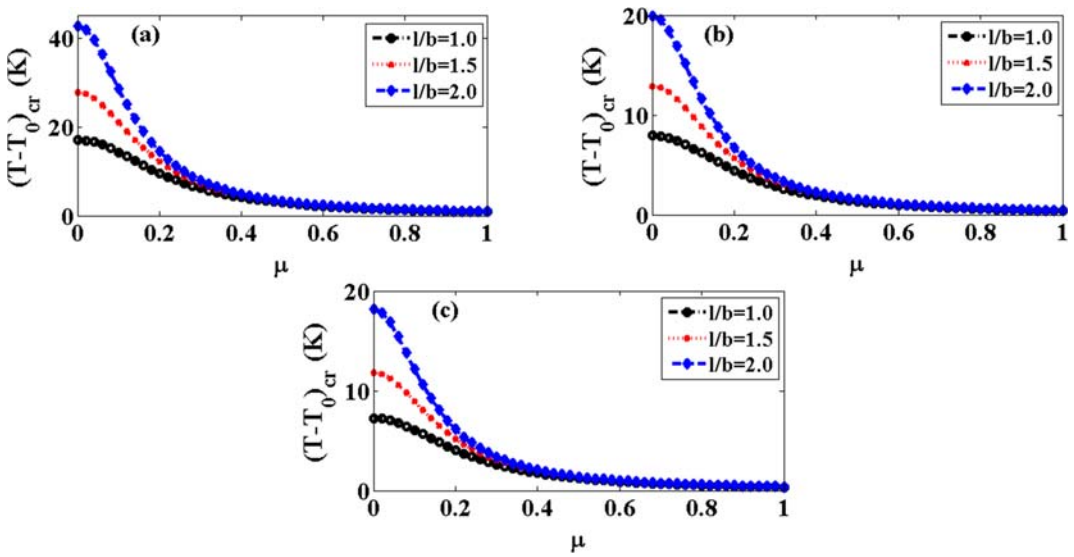

Fig. 5 Effect of the nonlocal parameter on the critical buckling temperature of a thin SSSS functionally graded nanoplate subjected to uniform temperature distribution (UTD) for different aspect ratios, $h/l = 0.01$, for **a** $n = 0$, **b** $n = 1$, and **c** $n = 5$

maximum loading is obtained for a slope of zero and decreases linearly for positive values of γ_1 and/or γ_2.

Buckling behavior of the FG rectangular nanoplate under various thermal loads for different nonlocal parameters, volume fraction exponents, and aspect ratios

The influence of different types of temperature distribution on the variations of the critical mechanical buckling load of the SSSS FG nanoplate with respect to the nonlocal parameter is shown in Fig. 7 for three power law indices. In this case, the temperature difference of $T_c - T_m = -10\ (K)$ in both LTD and NLTD cases. According to the former discussions, the nonlocal parameter and the power law index induce softening effect on the buckling behavior of the FG nanoplate under various temperature gradients in the z direction. However, varying the nonlocal parameter does not greatly change the critical buckling load for high values of the power law indices. Furthermore, the obtained results confirm that the buckling load is significantly affected by the type of the temperature distribution along the thickness of the FG nanoplate. Inspecting the plotted curves in Fig. 7, it is noted that the assumption of nonlinear temperature gradient across the nanoplate thickness estimates the smallest values for the critical mechanical buckling load, and the uniform temperature

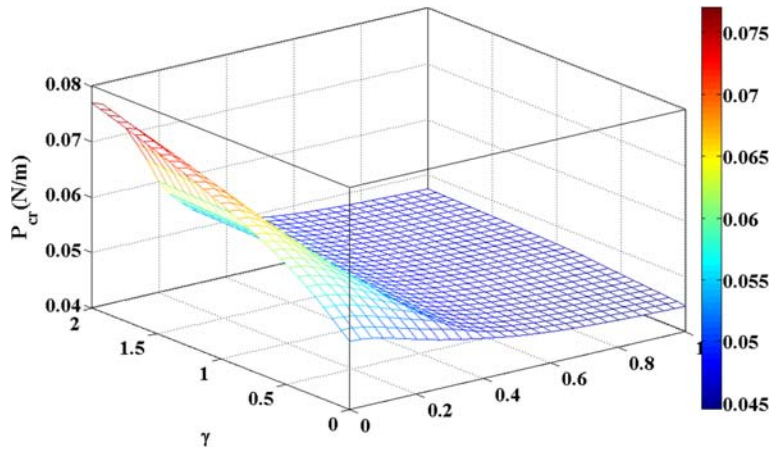

Fig. 6 Variation of the critical mechanical buckling load in terms of the nonlocal parameter and the slope of the linear mechanical load in the x direction for a thin SSSS FG nanoplate subjected to bi-axial compressive loads and uniform temperature distribution (UTD), $h = 0.34$ nm, $n = 1$, $\lambda = 0.5$, $\zeta_1 = -1$, $\zeta_2 = -1$, $\gamma_2 = 0.2$, and $T_c - T_m = -30\ (K)$.

distribution yields the highest critical mechanical buckling loads of the FG nanoplate. This result can be explained due to the fact that the average temperature of the nanoplate has the highest value in the case of nonlinear distribution of temperature. Indeed, an increase in the mean value of the temperature is accompanied by a reduction in the rigidity, and hence, the mechanical load required to buckle the FG nanoplate decreases. Note that the differences between the critical mechanical load of linear and nonlinear temperature distributions for larger values of the power law index are considerably higher than those for smaller gradient indices.

In Fig. 8, the critical buckling load versus the nonlocal parameter is depicted for the SSSS FG nanoplate subjected to three types of temperature distributions with various values of the slopes of the biaxial linearly varying mechanical loads γ_1 and γ_2. As mentioned before, for all three cases, when the nonlocal parameter of the FG nanoplate increases, the critical buckling load decreases. Besides, in all three cases of temperature gradient, it is noted that as the slopes of the linearly distributed forces increase, the values of the mechanical buckling load get larger. This is due to the fact that augmenting the factors γ_1 and γ_2 reduces the average value of the mechanical force, and hence, higher values of the initial mechanical load are needed to buckle the nanoplate. However, it is clear that by the continuous rise of the nonlocal parameter, the effect of the slopes γ_1 and γ_2 on the critical mechanical force cannot show itself for higher values of the nonlocal parameter. On the contrary, it is observed that by increasing the slopes for the linearly varying mechanical loads, the impact of the nonlocal parameter on the buckling behavior of the FG nanoplate would advance for all three types of temperature distribution. When the FG nanoplate experiences nonlinear temperature rise in the z direction, the lowest values of the mechanical buckling load are obtained due to the highest average temperatures and hence the smallest values of the FG nanoplate stiffness for that case. Moreover, it should be mentioned that the difference between the effect of uniform and linear temperature distributions is more noticeable than that between the impact of linear and nonlinear thermal gradients for all values of the nonlocal parameter and the slope of mechanical forces.

A comparison between the influence of linear and nonlinear temperature distributions on the variations of the critical mechanical load as a function of the temperature difference between the ceramic-rich and metal-rich surfaces $(\Delta T = T_c - T_m)$ of the FG nanoplate, with various boundary conditions, is shown in Fig. 9. As predicted, it can be found that the nonlinear temperature difference across the thickness of the FG nanoplate gives smaller values for mechanical buckling load compared with the linear temperature distribution for all values of ΔT. As explained earlier, this is because the nonlinear temperature distribution along the thickness

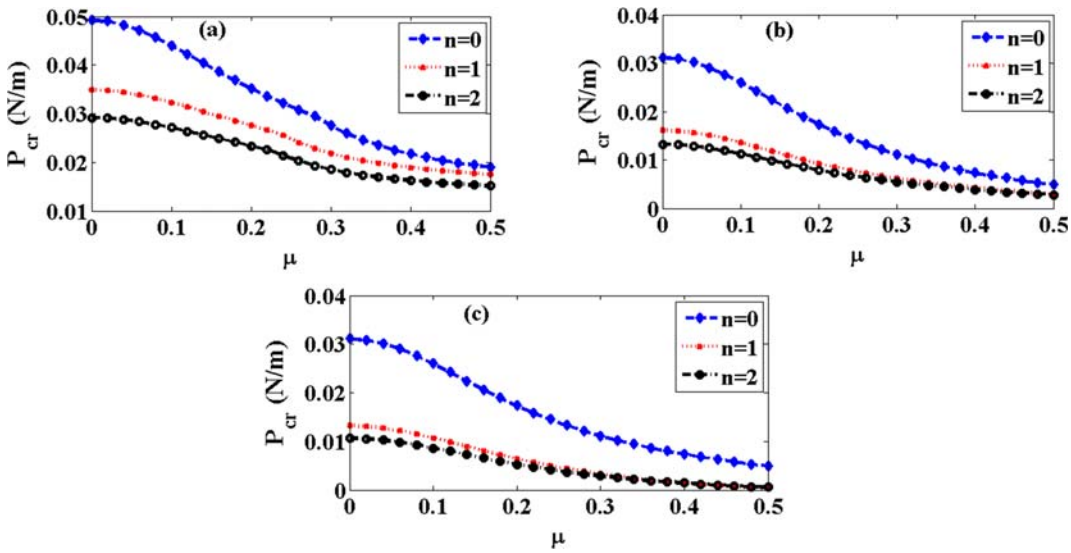

Fig. 7 Critical mechanical buckling load as a function of nonlocal parameter for a thin SSSS functionally graded nanoplate subjected to bi-axial compressive loads under linear temperature gradient with different power law indices, $h = 0.34$ nm, $h/l = 0.01$, $\zeta_1 = -1$, $\zeta_2 = -1$, $\gamma_1 = 0.5$, $\gamma_2 = 0.5$, $\lambda = 1$, for **a** UTD $T_c - T_m = 0$ (K), **b** LTD $T_c - T_m = -10$ (K), and **c** NLTD $T_c - T_m = -10$ (K)

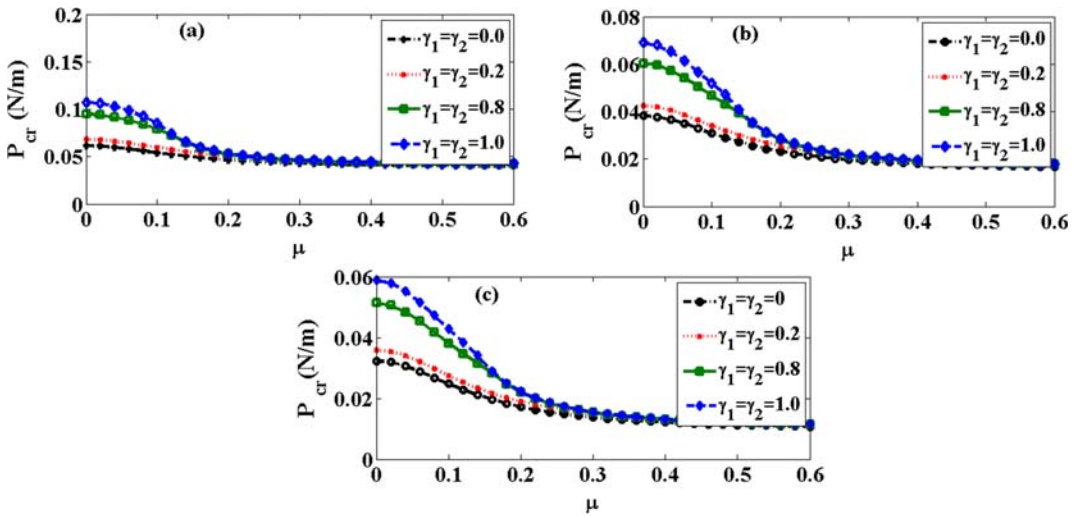

Fig. 8 Effect of the nonlocal parameter on the critical mechanical buckling load of a thin functionally graded SSSS nanoplate subjected to bi-axial compressive loads for different values of the slope of mechanical loads. h = 0.34 nm, h/l = 0.01, λ = 2, n = 2, $\zeta_1 = -1$, $\zeta_2 = -1$, **a** UTD $T_c - T_m = 0$ (K), **b** LTD $T_c - T_m = -30$ (K), and **c** NLTD $T_c - T_m = -30$ (K)

yields higher average temperatures, and subsequently, the critical mechanical load diminishes due to the softening behavior of temperature. In addition, the temperature difference across the thickness of the FG nanoplate can increase the critical mechanical load required for the nanoplate deflection. This is due to the fact that decreasing the ceramic side temperature with respect to the metallic surface temperature leads to stiffer the structure for both cases of temperature gradient (LTD and NLTD). Furthermore, in both cases (LTD and NLTD), it can be inferred that with increasing the number of clamped edges of the FG nanoplate, the resistance of the structure increases against deviation, and consequently, the critical mechanical load of the FG nanoplate improves significantly.

The impacts of the aspect ratio and the temperature distribution types on the variation of the critical mechanical buckling load with the temperature difference between the surfaces are illustrated in Figs. 10 and 11. As observed, by incrementing the temperature difference between the surfaces of the FG nanoplate, the value of the critical mechanical load required to buckle the plate would decrease for both thermal distributions (LTD and NLTD). This decrease results from decreasing the rigidity of the FG nanoplate due to the softening effect of the average temperature rise. It follows from the plotted

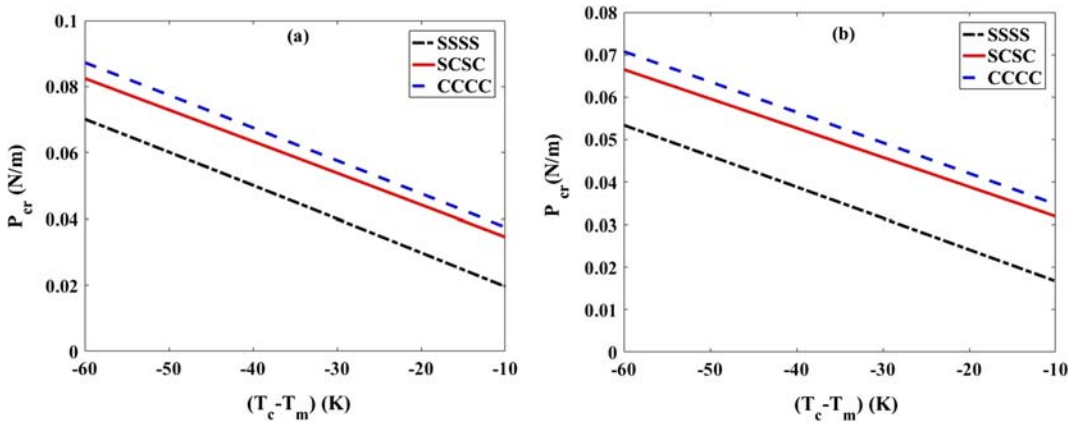

Fig. 9 Effect of the surface temperature difference on the critical buckling load of a thin functionally graded nanoplate subjected to bi-axial compressive loads and different boundary conditions, h = 0.34 nm, h/l = 0.01, μ = 0.1, λ = 1.5, n = 1, $\zeta_1 = -1$, $\zeta_2 = -1$, γ_1 = 0.5, and γ_2 = 0.5. **a** LTD. **b** NLTD

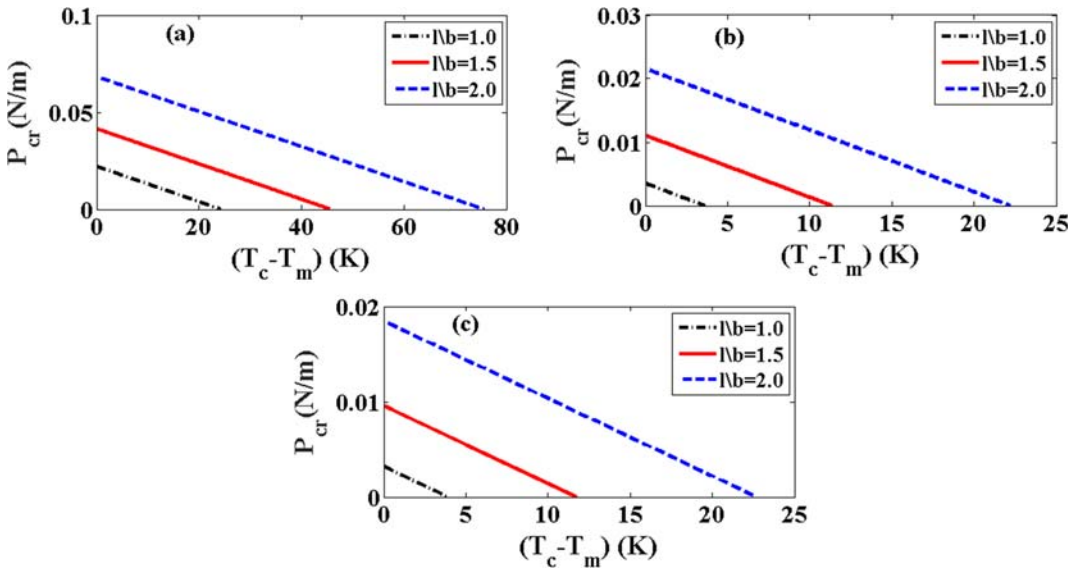

Fig. 10 Variation of the critical mechanical buckling load with respect to the temperature rise for a thin SSSS functionally graded nanoplate subjected to bi-axial compressive loads under linear temperature distribution (LTD) for different values of aspect ratio and power law index, $h/l = 0.01$, $\zeta_1 = -1$, $\zeta_2 = -1$, $\gamma_1 = 0.5$, $\gamma_2 = 0.5$, and $\mu = 0$. **a** $n = 0$. **b** $n = 2$. **c** $n = 5$

curves in Figs. 10 and 11 that the nonlinear temperature distribution reflects higher mechanical buckling loads compared with the linear temperature variation along the thickness of the FG nanoplate for $\Delta T > 0$. This means that the average temperature of the FG nanoplate for nonlinear temperature change is smaller than that of linear temperature gradient when the temperature of the ceramic-rich side is assumed to be higher than that of the metal-rich surface. Additionally, it is worthwhile to mention that as the aspect ratio increases, the critical mechanical force tends to increase for all values of the surface temperature difference under the two different temperature distributions (LTD and NLTD).

Finally, the variations of the critical buckling temperature of a SSSS FG nanoplate with the nonlocal parameter are shown in Fig. 12. Comparing Figs. 12a and b, it can be seen that for positive values of $T_c - T_m$, the assumption of linear temperature distribution estimates smaller values for the buckling surface temperature difference compared with the nonlinear temperature gradient across the thickness. Thus, for this case, the average temperature of the FG nanostructure related to the linear temperature distribution along the thickness is higher than that of nonlinear temperature change. Note that the difference between two cases increases for smaller values of nonlocal parameter. Moreover, it is shown that augmenting the nonlocal parameter reduces the critical temperature change across the thickness of the FG nanoplate, irrespective of the temperature gradient type, as predicted in the formulation of Eringen's nonlocal theory. This is expected since advancing the nonlocal parameter would decrease the interaction force between the nanoplate atoms, and that leads to a softer structure. The smaller the nonlocal parameter, the larger is the influence, regardless of the aspect ratio. Furthermore, it can be concluded that as the aspect ratio increases, the critical surface temperature difference of the FG nanoplate rises dramatically, where the aspect ratio was explained in Fig. 4. However, the gap between the curves diminishes with an increase in the nonlocal parameter; in other words, the increasing effect of the aspect ratio on the buckling temperature associated with the temperature difference along the z direction of the Cartesian coordinate system for the FG nanoplate vanishes after a certain value of the nonlocality nature index.

Conclusions

The thermo-mechanical buckling behavior of thin rectangular FG nanoplates subjected to biaxial linearly varying mechanical loads was investigated. Three different types of thermal loading were presented to investigate how different temperature distributions affect the overall response of the system. The small-scale effect

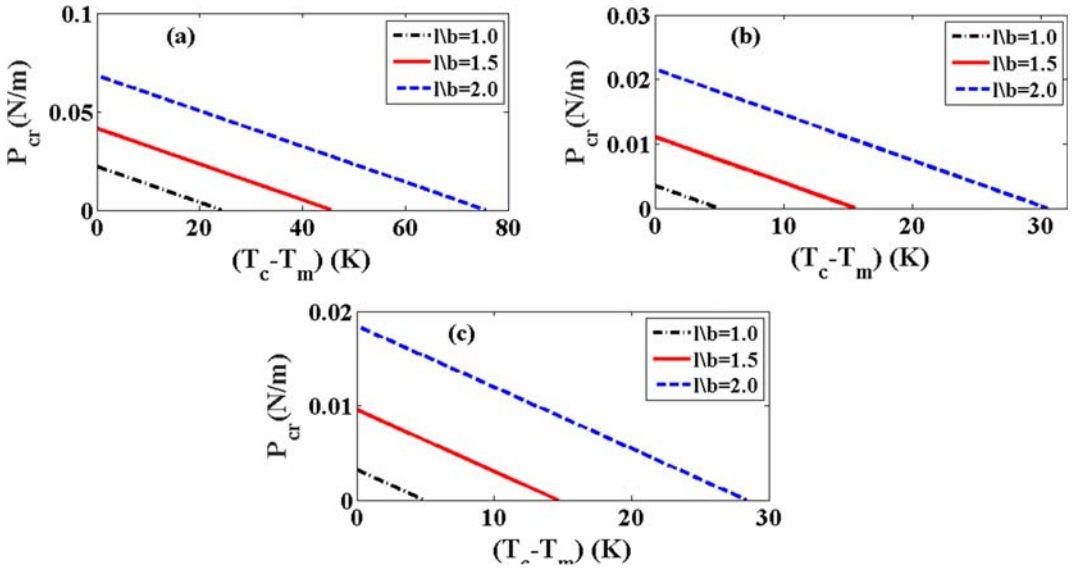

Fig. 11 Variation of the critical mechanical buckling load with respect to the temperature rise for a thin SSSS functionally graded nanoplate subjected to bi-axial compressive loads under nonlinear temperature distribution (NLTD) for different values of aspect ratio and power law index, $h/l = 0.01$, $\zeta_1 = -1$, $\zeta_2 = -1$, $\gamma_1 = 0.5$, $\gamma_2 = 0.5$,$\mu = 0$, **a** $n = 0$, **b** $n = 2$, and **c** $n = 5$

was taken into account by employing Eringen's nonlocal elasticity theory in the frame work of Kirchhoff's plate theory. A power-law function was utilized to describe the material properties. Implementing the minimum total potential energy principle, the governing equations of nanoplate were derived. Then, the Chebyshev spectral collocation method was applied to obtain the mechanical buckling loads and critical temperatures. Several numerical examples were provided to illustrate the impacts of the gradient index, the aspect ratio, the thermal distribution type, the nonlocal parameter, the slopes of the axial loads, and the boundary conditions on thermo-mechanical buckling behavior of thin FG nanoplates.

According to the results and findings, it is concluded that mechanical buckling load and critical temperature of FG nanoplates generally decrease with the increase of nonlocal parameter, while it improves with increasing the aspect ratio of the plate. Also, it is found that a way to increase the critical mechanical buckling load is to also increase the slopes of linearly varying mechanical forces. In addition, it was shown that the mechanical buckling load and the critical temperature difference for the FG nanoplate under linear temperature distribution across the thickness are smaller than the plates under nonlinear temperature distribution across the thickness for $\Delta T > 0$. On the contrary, as the temperature of metallic side becomes larger than the temperature of

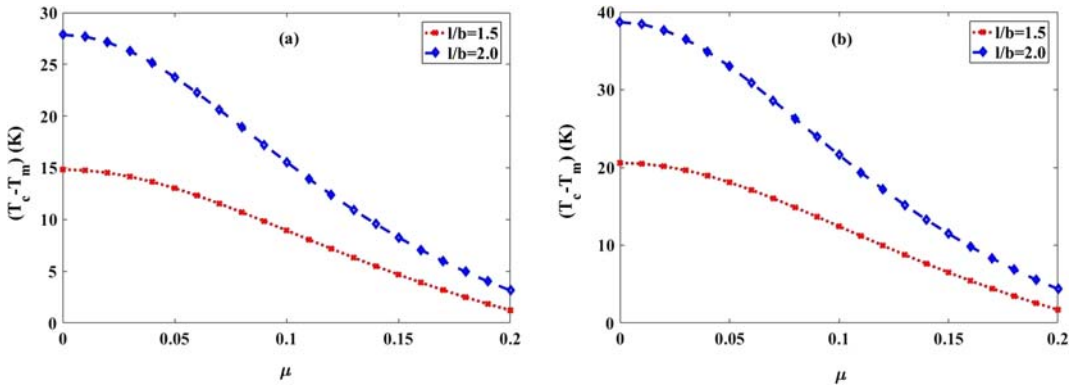

Fig. 12 Impact of the nonlocal parameter on the critical buckling temperature of a thin SSSS functionally graded nanoplate for two different aspect ratios, $h/l = 0.01$, $n = 1$. **a** LTD. **b** NLTD

ceramic surface, the buckling strength and the critical temperature for FG plates under nonlinear temperature gradient are smaller compared with the plates under linear temperature distribution. The proposed model was found to be appropriate and efficient method to analyze the buckling characteristics of thin nanostructures with graded compositions under both linearly varying mechanical loads and various types of temperature distributions.

Funding information This study is funded by the National Science Foundation Graduate Research Fellowship Program.

Compliance with ethical standards

Conflict of interest The authors declare that they have no conflicts of interest.

References

Akbarzadeh Khorshidi M, Shaat M, Abdelkefi A, Shariati M (2017) Nonlocal modeling and buckling features of cracked nanobeams with von Karman nonlinearity. Appl Physics A: Materials Science and Processing 123:62–12. https://doi.org/10.1007/s00339-016-0658-7

Akbaş ŞD (2017) Vibration and static analysis of functionally graded porous plates. *J Appl Comp Mech 3*(3):199–207. https://doi.org/10.22055/jacm.2017.21540.1107

Akgöz B, Civalek O (2013) Buckling analysis of functionally graded microbeams based on the strain gradient theory. Acta Mech 224:2185–2201

Akgöz B, Civalek O (2015) A microstructure-dependent sinusoidal plate model based on the strain gradient elasticity theory. Acta Mech 226:2277–2294

Ansari R, Gholami R (2016) Nonlocal free vibration in the pre- and post-buckled states of magneto-electro-thermo elastic rectangular nanoplates with various edge conditions. Smart Mater Struct 25(9):095033. https://doi.org/10.1088/0964-1726/25/9/095033

Arefi M, Mohammad-Rezaei Bidgoli E, Dimitri R, Tornabene F (2018) Free vibrations of functionally graded polymer composite nanoplates reinforced with graphene nanoplatelets. Aerosp Sci Technol 81:108–117. https://doi.org/10.1016/j.ast.2018.07.036

Ashoori AR, Sadough Vanini SA (2016) Thermal buckling of annular microstructure-dependent functionally graded material plates resting on an elastic medium. Compos Part B 87:245–255. https://doi.org/10.1016/j.compositesb.2015.10.024

Ashoori AR, Salari E, Sadough Vanini SA (2016) Size-dependent thermal stability analysis of embedded functionally graded annular nanoplates based on the nonlocal elasticity theory. Int J Mech Sci 119:396–411. https://doi.org/10.1016/j.ijmecsci.2016.10.035

Bakhsheshy A, Khorshidi K (2015) Free vibration of functionally graded rectangular nanoplates in thermal environment based on the modified couple stress theory. Modares Mech Eng 14:323–330

Barati MR, Shahverdi H (2016) A four-variable plate theory for thermal vibration of embedded FG nanoplates under non-uniform temperature distributions with different boundary conditions. *Struct Eng Mech 60*(4):707–727. https://doi.org/10.12989/sem.2016.60.4.707

Barati MR, Shahverdi H (2017) An analytical solution for thermal vibration of compositionally graded nanoplates with arbitrary boundary conditions based on physical neutral surface position. Mech Adv Mater Struct 24(10):840–853. https://doi.org/10.1080/15376494.2016.1196788

Barati MR, Zenkour AM, Shahverdi H (2016) Thermo-mechanical buckling analysis of embedded nanosize FG plates in thermal environments via an inverse cotangential theory. Compos Struct 141:203–212. https://doi.org/10.1016/j.compstruct.2016.01.056

Bouderba B, Houari MSA, Tounsi A (2013) Thermomechanical bending response of FGM thick plates resting on Winkler-Pasternak elastic foundations. *Steel Compos Struct 14*(1):85–104. https://doi.org/10.12989/scs.2013.14.1.085

Bouderba B, Houari MSA, Tounsi A, Mahmoud SR (2016) Thermal stability of functionally graded sandwich plates using a simple shear deformation theory. *Struct Eng Mech 58*(3):397–422. https://doi.org/10.12989/sem.2016.58.3.397

Bouiadjra RB, Adda Bedia EA, Tounsi A (2013) Nonlinear thermal buckling behavior of functionally graded plates using an efficient sinusoidal shear deformation theory. *Struct Eng Mech 48*(4):547–567. https://doi.org/10.12989/sem.2013.48.4.547

Bousahla AA, Benyoucef S, Tounsi A, Mahmoud SR (2016) On thermal stability of plates with functionally graded coefficient of thermal expansion. *Struct Eng Mech 60*(2):313–335. https://doi.org/10.12989/sem.2016.60.2.313

Chen J, Liu B, Yan L (2019) Nanoscale thermal transport in epoxy matrix composite materials reinforced with carbon nanotubes and graphene nanoplatelets. *J Nanopart Res* 21:256

Ebrahimi F, Barati MR (2016) Nonlocal thermal buckling analysis of embedded magneto-electro-thermo-elastic nonhomogeneous nanoplates. Iran J Sci Technol - Trans Mech Eng 40(4):243–264. https://doi.org/10.1007/s40997-016-0029-1

Ebrahimi F, Barati MR (2018) Vibration analysis of smart piezoelectrically actuated nanobeams subjected to magneto-electrical field in thermal environment. JVC/J Vib Control 24(3):549–564. https://doi.org/10.1177/1077546316646239

Ebrahimi F, Barati MR, Dabbagh A (2016a) A nonlocal strain gradient theory for wave propagation analysis in temperature-dependent inhomogeneous nanoplates. Int J Eng Sci 107:169–182. https://doi.org/10.1016/j.ijengsci.2016.07.008

Ebrahimi F, Ehyaei J, Babaei R (2016b) Thermal buckling of FGM nanoplates subjected to linear and nonlinear varying loads on Pasternak foundation. *Adv Mater Res 5*(4):245–261. https://doi.org/10.12989/amr.2016.5.4.245

Ebrahimi F, Salari E (2015) Nonlocal thermo-mechanical vibration analysis of functionally graded nanobeams in thermal environment. Acta Astronautica 113:29–50. https://doi.org/10.1016/j.actaastro.2015.03.031

El-Haina F, Bakora A, Bousahla AA, Tounsi A, Mahmoud SR (2017) A simple analytical approach for thermal buckling of thick functionally graded sandwich plates. *Struct Eng Mech 63*(5):585–595. https://doi.org/10.12989/sem.2017.63.5.585

Eringen AC (1983) On differential equations of nonlocal elasticity and solutions of screw dislocation and surface waves. J Appl Phys 54(9):4703–4710. https://doi.org/10.1063/1.332803

Eringen AC (2002) Nonlocal continuum field theories. Nonlocal continuum field theories. Springer, New York, New York. https://doi.org/10.1007/b97697

Farajpour MR, Shahidi AR, Farajpour A (2018) A nonlocal continuum model for the biaxial buckling analysis of composite nanoplates with shape memory alloy nanowires. Mater Res Express 5(3):035026. https://doi.org/10.1088/2053-1591/aab3a9

Gao Y, Xiao WS, Zhu H (2019) Nonlinear bending and thermal post-buckling behavior of functionally graded piezoelectric nanosize beams using a refined model. Mater Res Express 6(6):065065. https://doi.org/10.1088/2053-1591/ab0f78

Ghadiri M, Shafiei N, Akbarshahi A (2016) Influence of thermal and surface effects on vibration behavior of nonlocal rotating Timoshenko nanobeam. Appl Physics A: Materials Science and Processing 122:673–619. https://doi.org/10.1007/s00339-016-0196-3

Goodarzi M, Mohammadi M, Khooran M, Saadi F (2016) Thermo-mechanical vibration analysis of FG circular and annular nanoplate based on the visco-pasternak foundation. J Solid Mech 8(4):788–805

Hong CC (2014) Thermal vibration and transient response of magnetostrictive functionally graded material plates. Eur J Mech A/Solids 43:78–88. https://doi.org/10.1016/j.euromechsol.2013.09.003

Hosseini M, Bahreman M, Jamalpoor A (2017) Thermomechanical vibration analysis of FGM viscoelastic multi-nanoplate system incorporating the surface effects via nonlocal elasticity theory. Microsyst Technol 23(4):3041–3058. https://doi.org/10.1007/s00542-016-3133-7

Hosseini M, Jamalpoor A (2015) Analytical solution for thermomechanical vibration of double-viscoelastic nanoplate-systems made of functionally graded materials. J Therm Stresses 38(12):1428–1456. https://doi.org/10.1080/01495739.2015.1073986

Hosseini M, Jamalpoor A, Bahreman M (2016) Small-scale effects on the free vibrational behavior of embedded viscoelastic double-nanoplate-systems under thermal environment. Acta Astronautica 129:400–409. https://doi.org/10.1016/j.actaastro.2016.10.001

Javaheri R, Eslami MR (2002) Thermal buckling of functionally graded plates. AIAA J 40(1):162–169. https://doi.org/10.2514/3.15009

Jones RM (2006) Buckling of bars, plates, and shells. Bull Ridge Corporation, Biacksburg

Yuan Y, Zhao K, Sahmani S, & Safaei B (2020). Size-dependent shear buckling response of FGM skew nanoplates modeled via different homogenization schemes. Appl Math Mech 1-18.

Lori Dehsaraji M, Loghman A, & Arefi M (2020). Three-dimensional thermo-electro-mechanical buckling analysis of functionally graded piezoelectric micro/nano-shells based on modified couple stress theory considering thickness stretching effect. Mech Adv Mater Struct 1-16.

Żur KK, Arefi M, Kim J, Reddy JN (2020) Free vibration and buckling analyses of magneto-electro-elastic FGM nanoplates based on nonlocal modified higher-order sinusoidal shear deformation theory. Compos Part B 182:107601

Ruocco E, Reddy JN (2020) Buckling analysis of elastic–plastic nanoplates resting on a Winkler-Pasternak foundation based on nonlocal third-order plate theory. Int J Non-Linear Mech 121:103453

Guo J, Sun T, Pan E (2020) Three-dimensional nonlocal buckling of composite nanoplates with coated one-dimensional quasicrystal in an elastic medium. Int J Solids Struct 185:272–280

Karami B, Janghorban M, Li L (2018) On guided wave propagation in fully clamped porous functionally graded nanoplates. Acta Astronautica 143:380–390. https://doi.org/10.1016/j.actaastro.2017.12.011

Karami B, Shahsavari D, Li L, Karami M, Janghorban M (2019) Thermal buckling of embedded sandwich piezoelectric nanoplates with functionally graded core by a nonlocal second-order shear deformation theory. Proc Inst Mech Eng C J Mech Eng Sci 233(1):287–301. https://doi.org/10.1177/0954406218756451

Karimipour I, Tadi Beni Y, Akbarzadeh AH (2019) Size-dependent nonlinear forced vibration and dynamic stability of electrically actuated micro-plates. Commun Nonlinear Sci Numer Simul 78:104856

Karimi Zeverdejani M, Tadi Beni Y, Kiani Y (2020) Multi-scale buckling and post-buckling analysis of functionally graded laminated composite plates reinforced by defective graphene sheets. Int J Struct Stab Dyn 20:2050001

Khetir H, Bouiadjra MB, Houari MSA, Tounsi A, Mahmoud SR (2017) A new nonlocal trigonometric shear deformation theory for thermal buckling analysis of embedded nanosize FG plates. *Struct Eng Mech 64*(4):391–402. https://doi.org/10.12989/sem.2017.64.4.391

Kiani A, Sheikhkhoshkar M, Jamalpoor A, Khanzadi M (2018) Free vibration problem of embedded magneto-electro-thermo-elastic nanoplate made of functionally graded materials via nonlocal third-order shear deformation theory. J Intell Mater Syst Struct 29(5):741–763. https://doi.org/10.1177/1045389X17721034

Kiani Y, Bagherizadeh E, Eslami MR (2011) Thermal buckling of clamped thin rectangular FGM plates resting on Pasternak elastic foundation (three approximate analytical solutions). ZAMM Zeitschrift Fur Angewandte Mathematik Und Mechanik 91(7):581–593. https://doi.org/10.1002/zamm.201000184

Koizumi M (1997) FGM activities in Japan. Compos Part B 28(1–2):1–4. https://doi.org/10.1016/s1359-8368(96)00016-9

Kolahchi R, Bidgoli AMM, Heydari MM (2015) Size-dependent bending analysis of FGM nano-sinusoidal plates resting on orthotropic elastic medium. *Struct Eng Mech 55*(5):1001–1014. https://doi.org/10.12989/sem.2015.55.5.1001

Korayem MH, Khaksar H (2020) A survey on dynamic modeling of manipulation of nanoparticles based on atomic force microscope and investigation of involved factors. *J Nanopart Res* 22:27

Liu S, Yu T, Van Lich L, Yin S, Bui TQ (2019) Size and surface effects on mechanical behavior of thin nanoplates incorporating microstructures using isogeometric analysis. Comput Struct 212:173–187. https://doi.org/10.1016/j.compstruc.2018.10.009

Mahinzare M, Ranjbarpur H, Ghadiri M (2018) Free vibration analysis of a rotary smart two directional functionally graded piezoelectric material in axial symmetry circular nanoplate. Mech Syst Signal Process 100:188–207. https://doi.org/10.1016/j.ymssp.2017.07.041

Nami MR, Janghorban M, Damadam M (2015) Thermal buckling analysis of functionally graded rectangular nanoplates based on nonlocal third-order shear deformation theory. Aerosp Sci Technol 41:7–15. https://doi.org/10.1080/09243046.2014.901472

Norouzzadeh A, Ansari R, Rouhi H (2017) Pre-buckling responses of Timoshenko nanobeams based on the integral and differential models of nonlocal elasticity: an isogeometric approach. Appl Physics A: Materials Science and Processing 123:330. https://doi.org/10.1007/s00339-017-0887-4

Rahmani O, Jandaghian AA (2015) Buckling analysis of functionally graded nanobeams based on a nonlocal third-order shear deformation theory. Appl Physics A: Materials Science and Processing 119(3):1019–1032. https://doi.org/10.1007/s00339-015-9061-z

Sahmani S, Bahrami M, Ansari R (2014) Surface effects on the free vibration behavior of postbuckled circular higher-order shear deformable nanoplates including geometrical nonlinearity. Acta Astronautica 105(2):417–427. https://doi.org/10.1016/j.actaastro.2014.10.005

Saidi H, Houari MSA, Tounsi A, Bedia EAA (2013) Thermomechanical bending response with stretching effect of functionally graded sandwich plates using a novel shear deformation theory. *Steel Compos Struct 15*(2):221–245. https://doi.org/10.12989/scs.2013.15.2.221

Shahsavari D, Karami B, Mansouri S (2018) Shear buckling of single layer graphene sheets in hygrothermal environment resting on elastic foundation based on different nonlocal strain gradient theories. Eur J Mech A/Solids 67:200–214. https://doi.org/10.1016/j.euromechsol.2017.09.004

Sobhy M (2015) A comprehensive study on FGM nanoplates embedded in an elastic medium. Compos Struct 134:966–980. https://doi.org/10.1016/j.compstruct.2015.08.102

Sobhy M, Radwan AF (2017) A new quasi 3D nonlocal plate theory for vibration and buckling of FGM nanoplates. Int J Appl Mech 9(01):1750008. https://doi.org/10.1142/S1758825117500089

Zenkour AM (2011) A quasi-3D refined theory for functionally graded single-layered and sandwich plates with porosities. Compos Struct 201:38–48